Inclusion of wave steepening in a frequency-domain model of trombone sound production

Michael W. Thompson and William J. Strong
Department of Physics and Astronomy, Brigham Young University, Provo, Utah 84602

(Received 31 July 2000; revised 30 January 2001; accepted 21 March 2001)

A frequency-domain model of trombone sound production that includes the effects of wave steepening is proposed. This model builds upon the work of Msallam *et al.* [Proceedings of the Institute of Acoustics **19**(5), 419–424 (1997)] by including thermoviscous wall losses in a more realistic manner, by applying wave steepening systematically to the entire instrument, and by making quantitative comparisons to the experimentally measured output of the same trombone that the model is based on. The trombone is approximated as a set of contiguous cylindrical tubes with superposition of incoming and outgoing waves in each cylinder and with continuity of pressure and flow at each cylinder junction. The far-field radiated pressure spectrum is calculated on the basis of the spectrum of a measured pressure wave in the mouthpiece. This calculation includes the effects of wave steepening for the outgoing wave in each cylinder. The equations describing the model are given. Mouthpiece spectra are processed both with and without the effects of wave steepening. The predicted far-field spectra are compared to the corresponding measured far-field spectra. In all cases analyzed, the inclusion of wave steepening greatly reduces the error between predicted and measured spectra. © *2001 Acoustical Society of America.* [DOI: 10.1121/1.1371759]

PACS numbers: 43.75.Fg [RDA]

I. INTRODUCTION

For several years, wave steepening has been known to be partially responsible for the typically bright timbre of loudly blown trombone tones. Beauchamp (1980) observed that differences in sound pressure levels between radiated harmonics and corresponding harmonics in the mouthpiece are not constant for all dynamics, as a linear model would predict. An example of such a nonlinear response is shown in Fig. 1, where the divergence of the two curves is the result of amplitude-dependent behavior.

Hirschberg *et al.* (1996), documented shock waves at the bell of the trombone using a flow visualization technique. They also suggested that the change in timbre due to this observed wave steepening could be modeled by calculating the outgoing pressure wave in the mouthpiece based on linear theory, steepening the outgoing wave appropriately, and filtering the wave with a linear model of the horn to obtain the radiated pressure.

Msallam *et al.* (1997), developed a simple time-domain model that includes wave steepening in the slide of the trombone. The slide was treated as a single 3 m long cylindrical tube, and thermoviscous losses at the walls of the slide were applied prior to the wave steepening calculation. This simplified method of handling wall losses may have been adopted in order to avoid the numerous convolution sums encountered if the slide had been treated instead as a set of many shorter elements. To obtain the radiated sound, the steepened wave was processed by a linear filter representing the bell. Although their results were encouraging, Msallam *et al.*, did not quantitatively compare the output of their model to that of a real instrument.

The present research attempts to build on the work of Msallam *et al.*, by exploring the effect of wave steepening on sustained trombone tones in the frequency domain, both computationally and experimentally. Thermoviscous losses are more easily handled in the frequency domain, allowing the slide to be broken up into many smaller elements without incurring excessive computational load. Also, wave steepening is more systematically applied throughout the entire instrument—not just in the slide. A model has been developed that predicts well the radiated spectrum of the trombone at several combinations of dynamic and pitch. The output of the model is compared to experimentally measured tones from the same trombone that the model is based on, with good success.

II. THE FREQUENCY-DOMAIN MODEL

The instrument being modeled was a King Cleveland 605 tenor trombone with a Vincent Bach 12C mouthpiece. The shape of the instrument was approximated with a set of 152 cylindrical tubes; the lengths and radii of the cylinders were varied to provide a match to the trombone bore (Plitnik and Strong, 1979). All dimensions except those of the mouthpiece were taken from Copley's previous work (1995) on the same trombone. (Detailed dimensions are available in Appendix I of Thompson, 2000.)

A frequency-domain model of sound production was derived by considering lossy wave propagation in the cylinders and pressure reflection at the cylinder junctions. Since only steady, periodic waves were considered, the waves were represented as sums of harmonic components. Various parameters, including reflection coefficients and impedances, were specified only at harmonic frequencies. (A detailed derivation of the model is given in Appendices C and D of Thompson, 2000.)

Throughout this paper, the model is called linear when wave steepening is ignored and nonlinear when wave steep-

 0001-4966/2001/110(1)/556/7/$18.00

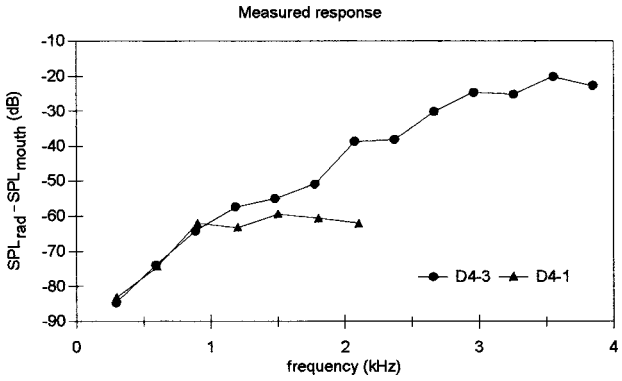

FIG. 1. Difference between measured radiated SPLs (see Figs. 3 and 4) and measured mouthpiece SPLs (see Fig. 2) at the pitch D4. D4-3 is a loud tone and D4-1 is a soft tone. The divergence of the two curves is evidence of amplitude-dependent behavior. Only values at harmonic frequencies are included.

ening is included. Also, a time dependence of $e^{j\omega t}$ is assumed throughout and has been omitted in order to simplify the notation.

A. The linear model

The equations for the linear model are given for a single frequency to simplify the notation. The subscript n refers to cylinder number, where $1 \leqslant n \leqslant N$ and $N=152$.

The trombone can be characterized acoustically in terms of the complex pressure reflection coefficients at the input ends (the ends nearest to the mouthpiece) of the cylinders. At the input of a given cylinder, the reflection coefficient is

$$R_n = \frac{P_n^-}{P_n^+}, \tag{1}$$

where P_n^+ and P_n^- are the outgoing and incoming complex pressure amplitudes, which can be treated as complex Fourier coefficients. Let us also define a dimensionless input impedance

$$Z_n' = \frac{A_{n-1}k_{n-1}}{\rho_0 \omega} Z_n, \tag{2}$$

where Z_n is the acoustic input impedance, A_{n-1} and k_{n-1} are the cross-sectional area and complex wave number of the adjacent cylinder nearest to the mouthpiece, ρ_0 is the ambient density of air, and ω is the angular frequency. At the junction of two cylinders, pressure and flow are continuous, which implies that acoustic impedance is also continuous. From these conditions (and after some algebra), the following equations can be obtained:

$$R_n = e^{-2jk_nL_n}\left(\frac{Z_{n+1}'-1}{Z_{n+1}'+1}\right) \tag{3}$$

and

$$Z_n' = \frac{A_{n-1}k_{n-1}}{A_n k_n}\left(\frac{1+R_n}{1-R_n}\right), \tag{4}$$

where L_n is the cylinder length. The dimensionless radiation impedance at the bell is

$$Z_{N+1}' = \frac{A_N k_N}{\rho_0 \omega} Z_{\text{bell}}, \tag{5}$$

where Z_{bell} is the acoustic radiation impedance of an unbaffled, plane circular piston in the end of a long cylindrical tube (Beranek, 1996). The reflection coefficients of all cylinders can be obtained by starting with Eq. (5) at the bell and alternately calculating Eqs. (3) and (4) back to the mouthpiece.

An experimentally measured pressure wave in the mouthpiece serves as the input to the model. Let the subscript ''mouth'' represent the index of the cylinder whose input end is nearest to the position where the mouthpiece pressure is known, and let P_{mouth} be a complex Fourier coefficient of the measured pressure wave. This Fourier coefficient can be separated into outgoing and incoming parts using linear theory. The outgoing pressure in the mouthpiece is

$$P_{\text{mouth}}^+ = \frac{P_{\text{mouth}}}{1+R_{\text{mouth}}}, \tag{6}$$

and the outgoing pressure at each of the subsequent cylinder inputs is

$$P_{n+1}^+ = P_n^+ e^{-jk_nL_n}\left(\frac{1+R_n e^{2jk_nL_n}}{1+R_{n+1}}\right). \tag{7}$$

Equation (7) is calculated repeatedly to model the filtering that occurs as the outgoing wave propagates through each cylinder in the model. The total pressure at the bell is

$$P_{\text{bell}} = P_N^+ e^{-jk_NL_N}\left(\frac{2Z_{N+1}'}{Z_{N+1}'+1}\right). \tag{8}$$

At a sufficiently large distance from the bell, the on-axis pressure is approximately equal to the pressure that would be radiated by a simple source having the same source strength. The radiated pressure can be expressed in terms of the total pressure at the bell and the radiation impedance as

$$P_{\text{rad}} = \frac{P_{\text{bell}}}{Z_{\text{bell}}}\frac{j\rho_0\omega}{4\pi x_{\text{rad}}}\exp\left(-j\frac{\omega}{c_0}x_{\text{rad}}\right), \tag{9}$$

where x_{rad} is the distance from the plane of the bell, and c_0 is the sound speed in air. From these predicted Fourier coefficients, the far-field radiated pressure wave can be synthesized.

B. Inclusion of wall losses

Thermoviscous losses at the walls of the cylinders can be included if we allow the wave number to be complex valued (Kinsler *et al.*, 1982):

$$k_n = \frac{\omega}{c_n} - j\alpha_n, \tag{10}$$

where

$$\alpha_n = \frac{1}{r_n c_0}\sqrt{\frac{\eta_{\text{eff}}\omega}{2\rho_0}} \tag{11}$$

and

$$c_n = c_0\left(1 - \frac{1}{2r_n}\sqrt{\frac{2\eta_{\text{eff}}}{\rho_0\omega}}\right) \tag{12}$$

are the attenuation coefficient and sound speed associated with these losses. In these expressions, r_n is the cylinder radius; and

$$\eta_{\text{eff}} = \eta\left[1 + (\gamma - 1)\sqrt{\frac{\kappa}{C_P\eta}}\right]^2 \tag{13}$$

is an effective viscosity, where η is the shear viscosity of air, γ is the adiabatic constant of air, κ is the thermal conductivity of air, and C_P is the specific heat of air at constant pressure.

C. The nonlinear model

The discussion of wave steepening that follows applies to the case of an outgoing wave in a single cylinder; the cylinder number index, *n*, is omitted and a harmonic number index, *h*, is used instead to handle the nonlinear interaction of harmonics, where $1 \leqslant h \leqslant H$ and $H = 200$. The choice of 200 harmonics was somewhat arbitrary and limited by the available computational resources. A much greater number of harmonics would be required in order to accurately model shock formation.

The Burgers equation predicts the wave steepening that occurs as an outgoing pressure wave propagates through each cylinder in the linear model. In the frequency domain, this equation is (Ginsberg and Hamilton, 1998; Appendix D of Thompson, 2000)

$$\frac{d}{dx}P_h^+ = -\frac{\delta\omega_h^2}{2c_0^3}P_h^+ + \frac{\beta\omega_k}{\rho_0 c_0^3}\frac{j}{4}\left\{\sum_{h'=1}^{h-1}(P_{h'}^+ P_{h-h'}^+) + 2\sum_{h'=h+1}^{\infty}[P_{h'}^+(P_{h'-h}^+)^*]\right\}, \tag{14}$$

where x is the distance from the input end of the cylinder; ω_h is the angular frequency of harmonic h;

$$\delta = \frac{1}{\rho_0}\left(\frac{4}{3}\eta + \eta_B\right) + \frac{\kappa}{\rho_0}\left(\frac{1}{C_V} - \frac{1}{C_P}\right) \tag{15}$$

is the diffusivity of sound (Hamilton and Morfey, 1998), where η_B is the bulk viscosity of air, and C_V is the specific heat of air at constant volume;

$$\beta = \frac{\gamma + 1}{2} \tag{16}$$

is the coefficient of nonlinearity; and * represents the complex conjugate. The first term on the right-hand side of Eq. (14) is proportional to the attenuation in the bulk of the fluid (Ginsberg and Hamilton, 1998),

$$\theta_h = \frac{\delta\omega_h^2}{2c_0^3}, \tag{17}$$

which reduces the amplitudes of the high-frequency harmonics as they increase due to wave steepening. The second term on the right-hand side of Eq. (14) is inversely related to the shock formation distance (Blackstock *et al.*, 1998)

$$x_{\text{shock}} = \frac{\rho_0 c_0^3}{\beta \max\left[\frac{d}{dt}p_{\text{mouth}}^+(t)\right]}. \tag{18}$$

The shock formation distance is inversely related to frequency and to acoustic pressure amplitude through the maximum value of the time derivative of the outgoing mouthpiece pressure wave in the denominator. This frequency dependence appears in the second term on the right-hand side of Eq. (14) as ω_h, and the amplitude dependence appears in the sums as pressure squared. The nonlinearities described by this equation are maximal at large pressure amplitudes and at high frequencies, or equivalently, at small shock formation distances.

It should be noted that Eq. (14) accounts for changes in the outgoing Fourier coefficients due only to wave steepening and thermoviscous losses in the bulk of the fluid; phase change due to propagation and losses at the wall of the cylinder were already included in Eq. (7). Wall and bulk losses are handled asymmetrically because wall losses are best applied to both the outgoing and the incoming waves via the complex wave number, while bulk losses are needed in the steepening of the outgoing wave in order to control the amplitude of the high-frequency harmonics during shock formation.

A good numerical method for solving Eq. (14) is fourth order Runge–Kutta. Since this method requires real equations of real variables, this equation must be separated into real and imaginary components:

$$\frac{d}{dx}X_h = -\theta_h X_h - \phi_h\left[\sum_{h'=1}^{h-1}(X_{h'}Y_{h-h'} + Y_{h'}X_{h-h'}) + 2\sum_{h'=h+1}^{H}(Y_{h'}X_{h'-h} - X_{h'}Y_{h'-h})\right] \tag{19}$$

and

$$\frac{d}{dx}Y_h = -\theta_h Y_h + \phi_h\left[\sum_{h'=1}^{h-1}(X_{h'}X_{h-h'} - Y_{h'}Y_{h-h'}) + 2\sum_{h'=h+1}^{H}(X_{h'}X_{h'-h} + Y_{h'}Y_{h'-h})\right] \tag{20}$$

where the substitutions

$$X_h + jY_h = P_h^+ \tag{21}$$

and

$$\phi_h = \frac{\beta\omega_h}{\rho_0 c_0^3}\frac{1}{4} \tag{22}$$

have been made to simplify the notation, and the Fourier series has been truncated at H harmonics.

Wave steepening can be included in the linear algorithm as follows: At the input of the cylinder in the mouthpiece where the measured pressure wave is known, the outgoing pressure coefficients are computed from Eq. (6). If desired, the shock formation distance can then be computed from Eq.

(18). The maximum value of the time derivative in this equation is best obtained by evaluating the analytical time derivative of the Fourier synthesis equation using a large number of samples per period and taking the maximum sample value. The outgoing mouthpiece pressure coefficients are modified by Eqs. (19) and (20), which models the wave steepening that would result from a propagation distance equal to the length of the cylinder. In this calculation, the algorithm is allowed to take a maximum spatial step of 5% of the shock formation distance in order to prevent large numerical error. Equation (7) is then computed to account for phase change, losses at the wall, and filtering at the cylinder junction. The process is repeated for each cylinder in the model. After wave steepening has been calculated for the final cylinder at the bell, the pressures at the bell and in the far field are computed from Eqs. (8) and (9).

Although the superposition of outgoing and incoming waves is not strictly valid for a nonlinear system, Msallam *et al.* (1997) concluded that errors due to this oversight would be less than 5% for harmonics below the 30th. They also reported that steepening the incoming wave did not significantly affect their results. This supports the suggestion of Hirschberg *et al.* (1996), that the gain in high-frequency energy due to wave steepening is mostly radiated at the bell, implying that steepening need be calculated for only the outgoing wave.

D. Testing the model

Several tests were performed to determine the reliability of the model; each test confirmed that the model was properly implemented. Errors on the order of a few dB are tolerable since the phenomenon of interest—the gain in high-frequency energy due to wave steepening—is on the order of tens of dB (see Fig. 1).

The input impedances of three theoretical tube shapes—a cylindrical pipe, a conical horn, and an exponential horn—were calculated based on approximations using sets of contiguous cylinders. The impedance magnitudes and phases were compared to the analytical results (Fletcher and Rossing, 1991) with good agreement. The error in the cylindrical case was negligible. The exponential case had the largest error—on the order of a few dB for frequencies below 20 kHz when using 150 cylinders. Admittedly, a more accurate (and mathematically complex) model could be implemented using cones instead of cylinders.

The input impedance of the trombone at the mouthpiece was calculated and compared to measured and calculated results from a different model of the same instrument (Copley, 1995). The resonance frequencies and corresponding impedance magnitudes agreed well.

Wave steepening of a sinusoid was calculated over one shock formation distance using 10 and 20 spatial steps. The differences in harmonic amplitudes between the two cases were a fraction of a dB. This suggests that allowing a maximum spatial step of 5% of the shock formation distance keeps the numerical error of the Runge–Kutta algorithm within acceptable limits.

III. EXPERIMENTAL VERIFICATION

A. Collecting the data

The model was thoroughly tested with experimentally measured tones from the same trombone that the model is based on. In an anechoic chamber, the trombone was mounted at a comfortable height for playing, with the bell oriented horizontally. The diaphragm of a PCB 112A23 microphone was mounted flush with the inside wall of the mouthpiece by means of a hole drilled through the wall. The signal from this microphone was recorded to one channel of a digital audio tape. A 1/2″ Larson–Davis 2540 microphone was mounted on-axis 2.85 m in front of the bell, and the signal from this microphone was recorded to the second channel of the tape. The bandwidth of the Larson–Davis microphone is approximately 20 Hz to 20 kHz, and the usable bandwidth of the PCB microphone was measured to be approximately 100 Hz to 16 kHz. Both microphones were calibrated so that accurate pressure values could be obtained from the recorded data. Sustained tones were recorded at the pitches B♭2, F3, B♭3, and D4 at various dynamics. The sample rate was 44.1 kHz. (Details of the experimental apparatus, calibration, and procedure can be found in Appendix G of Thompson, 2000.)

B. Preparing and processing the data

Six tones at the lowest pitch and three tones at each of the other pitches were chosen for analysis. These tones ranged from the softest to the loudest that the player could produce comfortably. Each of the tones was labeled with its pitch name and octave number and with a number representing the dynamic at which it was played. The dynamics were numbered in increasing order, from soft to loud. For example, the tone D4-1 is the softest tone analyzed at the pitch D in the fourth octave.

A steady segment of 10 periods was extracted from each of the B♭2 tones. The numbers of periods extracted from the tones at the other pitches (see Table I) were chosen so that all segments had approximately the same duration ($\sim$ 8.5 ms). The measured fundamental frequencies (see Table I) of these tones agreed well with the fundamental frequencies predicted by linear theory (Copley, 1995), and were therefore used in the model computations. The complex Fourier coefficients of the mouthpiece and the far-field radiated waves of each segment were calculated. Because all harmonics above a certain frequency (see Table I) had amplitudes less than the noise floor, data above that frequency were discarded. Figure 2 shows the mouthpiece spectra for the tones D4-1 and D4-3.

The Fourier series of each segment of mouthpiece data was processed by the model to predict the measured pressure at the far-field location. Each tone was processed twice—once neglecting wave steepening and once including wave steepening. The shock formation distances (see Table I), the SPLs of all Fourier coefficients (relative to 20 μPa), the errors in SPLs between the measured and predicted far-field coefficients, and the synthesized far-field pressure waves were calculated for all tones. (Complete experimental and computational data are given in Appendix H of Thompson, 2000.)

TABLE I. Tone parameters. The shock formation distances [see Eq. (18)] were computed from the outgoing mouthpiece pressures. For comparison, the length of the trombone is 2.72 m. The mouthpiece signal cutoff frequencies were the frequencies above which noise in the mouthpiece signal prevented accurate estimation of the harmonic amplitudes. They are also the maximum frequencies used in computing the errors in Fig. 7.

Tone	Fundamental frequency (Hz)	Number of periods analyzed	Shock formation distance (m)	Mouthpiece signal cutoff frequency (kHz)
B♭2-1	116.98±0.04	10	44	0.936
B♭2-2	117.07±0.04	10	11	1.874
B♭2-3	118.90±0.04	10	4.5	2.735
B♭2-4	119.58±0.04	10	3.0	2.990
B♭2-5	118.68±0.04	10	2.0	4.154
B♭2-6	117.04±0.04	10	0.90	4.916
F3-1	177.68±0.05	15	34	1.422
F3-2	177.16±0.05	15	3.3	2.658
F3-3	176.78±0.05	15	1.5	3.182
B♭3-1	238.83±0.07	20	20	1.672
B♭3-2	237.03±0.07	20	4.7	2.134
B♭3-3	235.51±0.07	20	1.5	3.298
D4-1	300.82±0.09	25	16	2.106
D4-2	297.65±0.09	25	3.4	2.679
D4-3	296.13±0.09	25	1.6	3.850

C. Selected results

The results from the softest and loudest tones at the pitch D4 (tones D4-1 and D4-3) typify the results obtained for all other tones. They will be used as examples in the discussion that follows.

Both the linear and the nonlinear models predict approximately the same radiated spectrum for the soft tone (see Fig. 3). In the case of the loud tone (see Fig. 4), however, the nonlinear model predicts the measured spectrum reasonably well, while the linear model severely underestimates the amount of high frequency energy in the measured spectrum.

A comparison of the measured and predicted pressure waves confirms the superiority of the nonlinear model. For the soft tone [see plots (b) through (d) of Fig. 5], the waves predicted by both models have amplitudes and phases similar to the measured wave. In the case of the loud tone [see plots (b) through (d) of Fig. 6], however, the nonlinear model predicts an amplitude that is reasonably correct, while the linear model predicts an amplitude that is much too small.

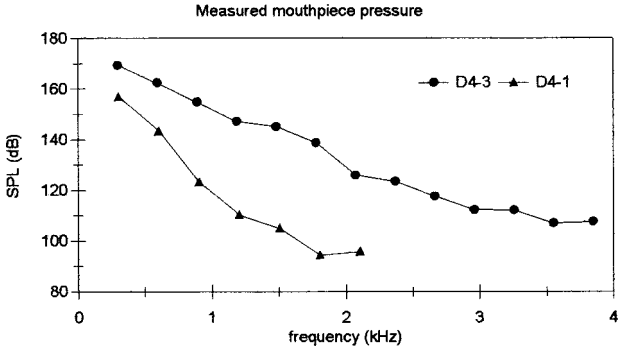

FIG. 2. Measured mouthpiece pressure spectra for the tones D4-1 and D4-3. Only values above the noise floor and at harmonic frequencies are included. Mouthpiece wave forms are shown in plots (a) of Figs. 5 and 6.

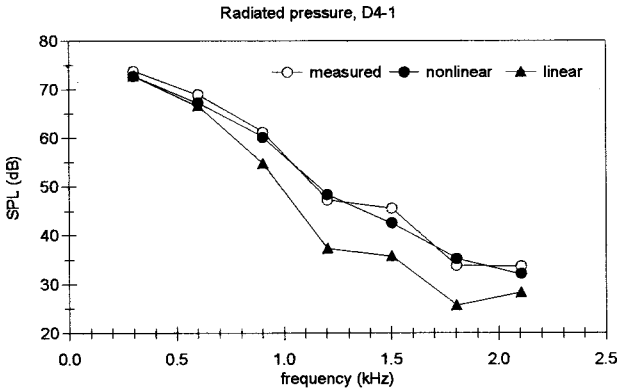

FIG. 3. Radiated pressure spectra for the tone D4-1. The SPLs predicted by the nonlinear and linear models are compared to the SPLs measured on-axis 2.85 m in front of the bell. Only values at harmonic frequencies are included. Radiated wave forms are shown in plots (b)–(d) of Fig. 5.

At extremely loud dynamics corresponding to shock formation distances significantly less than the length of the instrument, the nonlinear model tends to overestimate the amplitudes of the high-frequency harmonics. This problem has been reported previously for a similar computation (Anderson and Vaidya, 1991). This error is mostly due to the truncation of the Fourier series at 200 harmonics. Another contributing factor may be that the calculation of wave steepening and the calculation of wall losses are not done simultaneously for the outgoing wave in a given cylinder. This factor may be lessened by dividing the longest cylinders in the approximation into several shorter cylinders, thereby distributing the wall losses more uniformly.

Figure 7 compares the errors in SPLs from both models for all 15 tones. The nonlinear model clearly does better than the linear model at predicting the pressure at the far-field location. The anomalies in the data (i.e., B♭ 2-4 and F3-3) can be attributed to noise in the mouthpiece data that was not completely removed before processing.

In informal listening tests, the tones generated by the nonlinear model were found to be similar in timbre to the experimentally measured tones, but the tones generated by the linear model were found to be lacking in brightness.

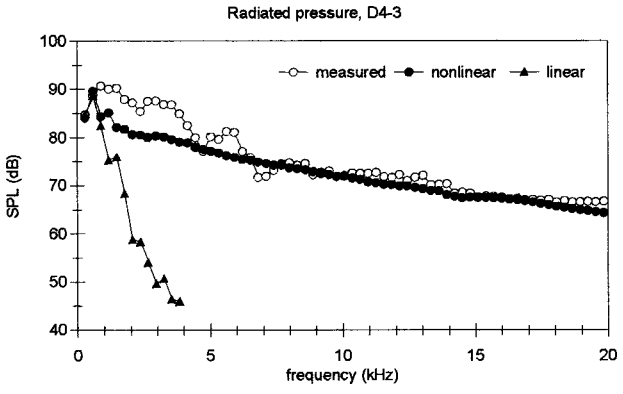

FIG. 4. Radiated pressure spectra for the tone D4-3. The SPLs predicted by the nonlinear and linear models are compared to the SPLs measured on-axis 2.85 m in front of the bell. Only values at harmonic frequencies are included. Radiated wave forms are shown in plots (b)–(d) of Fig. 6.

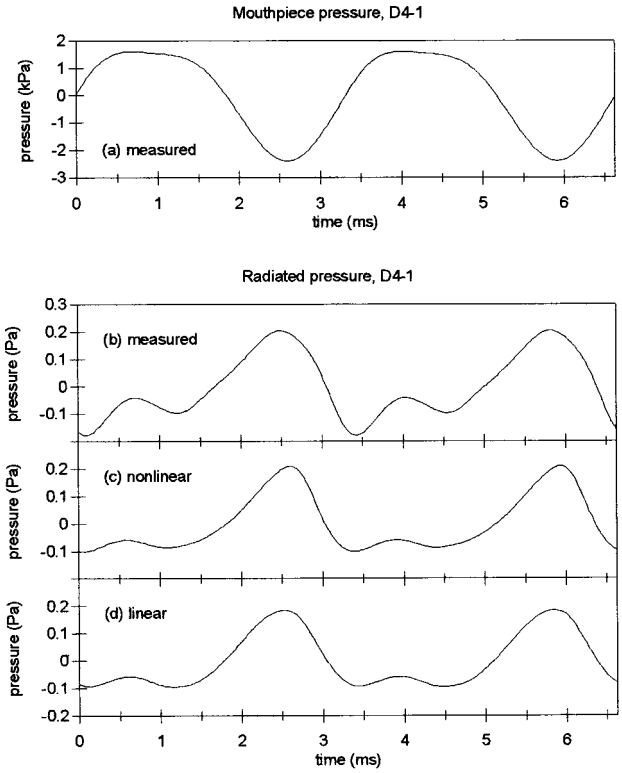

FIG. 5. Acoustic pressure wave forms for the tone D4-1. (a) Measured wave in the mouthpiece. (b) Measured wave on-axis 2.85 m in front of the bell. (c) Radiated wave computed from the nonlinear model. (d) Radiated wave computed from the linear model. DC offset has been neglected. The mouthpiece spectrum is shown in Fig. 2. The radiated spectra are shown in Fig. 3.

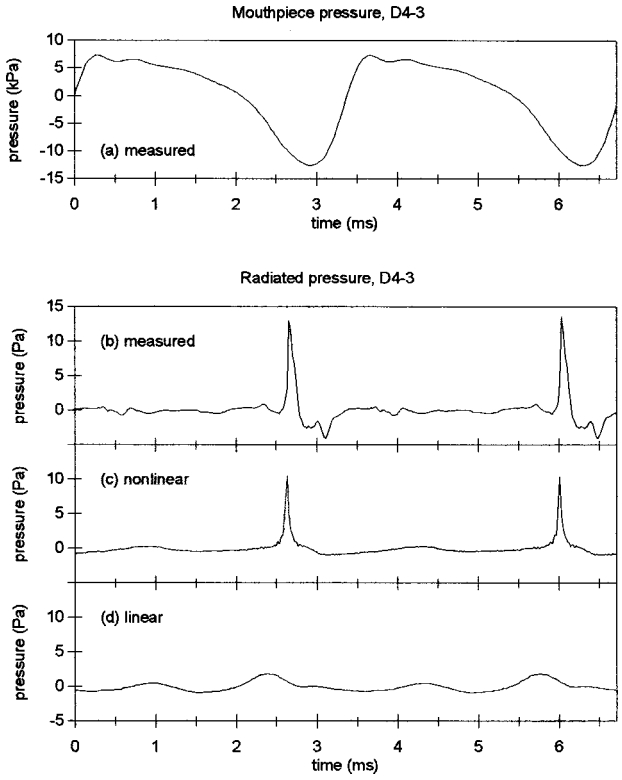

FIG. 6. Acoustic pressure wave forms for the tone D4-3. (a) Measured wave in the mouthpiece. (b) Measured wave on-axis 2.85 m in front of the bell. (c) Radiated wave computed from the nonlinear model. (d) Radiated wave computed from the linear model. DC offset and frequencies above 20 kHz have been neglected. The mouthpiece spectrum is shown in Fig. 2. The radiated spectra are shown in Fig. 4.

IV. CONCLUSIONS

The results are indeed encouraging. For small-amplitude tones, both the linear and the nonlinear models predict well the measured data. At large amplitudes, the nonlinear model is reasonably accurate in its predictions, while the linear model severely underestimates the amplitudes of the high-frequency harmonics. However, at shock formation distances significantly less than the length of the instrument, the nonlinear model tends to overestimate the amplitudes of the high-frequency harmonics.

The model may be improved upon by using a greater number of cylinders in the approximation, which would effectively distribute the losses at the walls of the cylinders more uniformly. Including more harmonics in the computation would help to reduce numerical error in the wave steepening calculation. Using mouthpiece data with a lower noise floor would permit evaluation of the model at higher frequencies. A more accurate model could be formulated using a set of contiguous cones instead of cylinders.

Although direct comparisons between the present research and the work of Msallam *et al.* (1997), cannot be made conclusively, this research builds upon their work by providing an alternate method for including wave steepening in a computational model of trombone sound production: Thermoviscous wall losses are handled in a more realistic manner, wave steepening is applied systematically to the entire instrument, and the accuracy of the model is analyzed

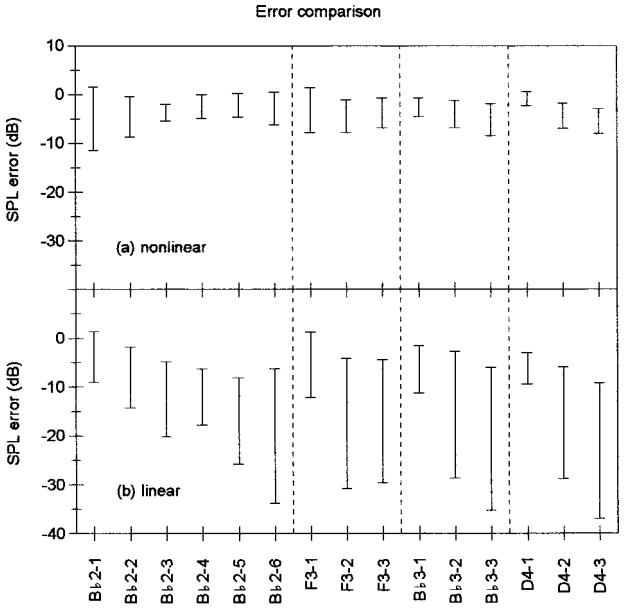

FIG. 7. Comparison of the average errors between measured and computed harmonic SPLs from both models. Each line ranges from the mean error in SPLs minus the standard deviation of the error to the mean plus the standard deviation. Only frequencies below the mouthpiece signal cutoff frequencies (see Table I) were included. The different dynamics at each pitch are numbered in increasing order, from soft to loud.

quantitatively through comparison of its output to experimentally measured tones.

ACKNOWLEDGMENTS

The trombone was played by Gordon Dix. This research was funded in part by a grant from the Institute for Scientific Research in Music.

APPENDIX A: VALUES OF PHYSICAL CONSTANTS

The following values were used for the physical constants that appear in the equations of the model. Approximations were made where precise values could not be determined. Although the values chosen may not perfectly reflect the conditions under which the experiment was conducted, a small change in any of the values does not significantly alter the computational results:

$$c_0 = 350\,\frac{\mathrm{m}}{\mathrm{s}}, \tag{A1}$$

$$C_P = 957.6\,\frac{\mathrm{J}}{\mathrm{kg\,K}}, \tag{A2}$$

$$C_V = \frac{C_P}{\gamma} = 683.0\,\frac{\mathrm{J}}{\mathrm{kg\,K}}, \tag{A3}$$

$$\beta = 1.201 \quad [\text{see Eq. (16)}], \tag{A4}$$

$$\gamma = 1.402, \tag{A5}$$

$$\delta = 3.80\times 10^{-5}\,\frac{\mathrm{m}^2}{\mathrm{s}} \quad [\text{see Eq. (15)}], \tag{A6}$$

$$\eta = 1.81\times 10^{-5}\ \mathrm{Pa\,s}, \tag{A7}$$

$$\eta_B = 0.6\,\eta = 1.09\times 10^{-5}\ \mathrm{Pa\,s}, \tag{A8}$$

$$\eta_{\mathrm{eff}} = 3.90\times 10^{-5}\ \mathrm{Pa\,s} \quad [\text{see Eq. (13)}], \tag{A9}$$

$$\kappa = 0.0234\,\frac{\mathrm{W}}{\mathrm{m\,K}}, \tag{A10}$$

$$\rho_0 = 1.18\,\frac{\mathrm{kg}}{\mathrm{m}^3}. \tag{A11}$$

Anderson, M. J., and Vaidya, P. G. (**1991**). ''Thermo-viscous effects on finite amplitude sound propagation in a rectangular waveguide,'' J. Acoust. Soc. Am. **90**, pp. 1056–1067.

Beauchamp, J. W. (**1980**). ''Analysis of simultaneous mouthpiece and output waveforms of wind instruments,'' Audio Engineering Society preprint No. 1626.

Beranek, L. L. (**1996**). *Acoustics*, 5th ed. (Acoustical Society of America, Woodbury, NY), pp. 116–128.

Blackstock, D. T., Hamilton, M. F., and Pierce, A. D. (**1998**). ''Progressive waves in lossless and lossy fluids,'' in *Nonlinear Acoustics*, edited by M. F. Hamilton and D. T. Blackstock (Academic, San Diego), pp. 65–76.

Copley, D. C. (**1995**). M. S. thesis, Brigham Young University.

Fletcher, N. H., and Rossing, T. D. (**1991**). *The Physics of Musical Instruments* (Springer-Verlag, New York), pp. 183–194.

Ginsberg, J. H., and Hamilton, M. F. (**1998**). ''Computational methods,'' in *Nonlinear Acoustics*, edited by M. F. Hamilton and D. T. Blackstock (Academic, San Diego), pp. 311–319.

Hamilton, M. F., and Morfey, C. L. (**1998**). ''Model equations,'' in *Nonlinear Acoustics*, edited by M. F. Hamilton and D. T. Blackstock (Academic, San Diego), pp. 53–54.

Hirschberg, A. J., Gilbert, J., Msallam, R., and Wijnands, A. P. J. (**1996**). ''Shock waves in trombones,'' J. Acoust. Soc. Am. **99**, 1754–1758.

Kinsler, L. E., Frey, A. R., Coppens, A. B., and Sanders, J. V. (**1982**). *Fundamentals of Acoustics*, 3rd ed. (Wiley, New York), pp. 206–210.

Msallam, R., Dequidt, S., Tassart, S., and Caussé, R. (**1997**). ''Physical model of the trombone including nonlinear propagation effects,'' Proceedings of the Institute of Acoustics, **19**(5), pp. 419–424.

Plitnik, G. R., and Strong, W. J. (**1979**). ''Numerical method for calculating input impedances of the oboe,'' J. Acoust. Soc. Am. **65**, 816–825.

Thompson, M. W. (**2000**). M. S. thesis, Brigham Young University.